Photophysics of cage/guest assemblies: photoinduced electron transfer between a coordination cage containing Os(II) luminophores, and electron-deficient bound guests in the central cavity.

Jennifer S. Train,[a] Ashley B. Wragg,[a] Alexander J. Auty,[a] Alexander J. Metherell,[a] Dimitri Chekulaev,[a] Christopher G. P. Taylor,[b] Stephen P. Argent,[b] Julia A. Weinstein,[*,a] and Michael D. Ward[*,b]

a Department of Chemistry, University of Sheffield, S3 7HF, UK.
Email: Julia.Weinstein@sheffield.ac.uk

b Department of Chemistry, University of Warwick, Coventry CV4 7AL, UK.
Email: m.d.ward@warwick.ac.uk

Abstract

A heterometallic octanuclear coordination cage $[Os_4Zn_4(L^{nap})_{12}]X_{16}$ (denoted **Os•Zn**; X = perchlorate or chloride) has been prepared (L^{nap} is a bis-bidentate bridging ligand containing two pyrazolyl-pyridine chelating units separated by a 1,5-naphthalene-diyl spacer group). The $\{Os(NN)_3\}^{2+}$ units located at four of the eight vertices of the cube have a long-lived, phosphorescent ^{3}MLCT excited state which is a stronger electron donor than $[Ru(bipy)_3]^{2+}$. The chloride form of **Os•Zn** is water soluble and binds in its central cavity the hydrophobic electron-accepting organic guests 1,2,4,5-tetracyanobenzene, 1,4-naphthoquinone and 1-nitronaphthalene, with binding constants in the range $10^3 – 10^4$ M^{-1}, resulting in quenching of the phosphorescence arising from the Os(II) units. A crystal structure of an isostructural Co_8 cage containing one molecule of 1,2,4,5-tetracyanobenzene as a guest inside the cavity has been determined. Ultrafast transient absorption measurements show formation of a charge-separated Os(III)/guest$^{\bullet-}$ state arising from cage-to-guest photoinduced electron transfer; this state is formed within 13 – 21 ps, and decays on a timescale of *ca.* 200 ps. In the presence of a competing guest with a large binding constant (cycloundecanone) which displaces each electron-accepting quencher from the cage cavity, the charge-separated state is no longer observed. Further, a combination of mononuclear $\{Os(NN)_3\}^{2+}$ model complexes with the same electron-accepting species showed no evidence for formation of charge-separated Os(III)/guest$^{\bullet-}$ states. These two control experiments indicate that the $\{Os(NN)_3\}^{2+}$ chromophores need to be assembled into the cage structure to bind the electron-accepting guests, and for PET to occur. These results help to pave the way for use of photoactive coordination cages as hosts for photo-redox catalysis reactions on bound guests.

Introduction

Coordination cages, in which a combination of metal ions and bridging ligands self-assemble into a hollow three-dimensional array with a well-defined central cavity, have been of particular interest for functions associated with binding of small molecule guests in the cavity.[1] In many cases this function relies simply on the structure of the host container molecule with the precise chemical nature of the component parts of the cage being of secondary importance: the cage is simply an inert box of given dimensions, solubility and charge. Examples of such systems are provided by the occurrence of many kinds of catalysed reactions of bound guests,[2] or the transport of drug molecules in cage cavities across cell membranes.[3] Both of these functions depend on the cavity characteristics of the host molecule but are generally independent of the specific chemical properties of the metal ions at the cage vertices which play a purely structural role.

In contrast to this well-established approach, there has been recent interest in the host/guest chemistry of coordination cages in which the components of the cage – either metal ions or bridging ligands – play a more active role in the functional behaviour, with the most obvious example being cage/guest systems that are photophysically active (*i.e.* they display luminescence, or there is an excited-state interaction such as photoinduced energy or electron transfer between host and guest).[4] Luminescent cages may have their emission properties modulated by guest binding, providing shape- and size-selective sensors for substrates as diverse as nitroaromatic compounds,[5] chemical warfare agent simulants,[6] or nucleosides.[7] The array of chromophores in a cage superstructure may also participate in photoinduced electron transfer with bound guests, leading to a range of photo-catalysed transformations in which the cage not only recognises and binds the substrate in the cavity, but acts as a photochemical reaction partner.[4a,8] This process offers a particularly appealing way to exploit the properties of coordination cages: the large number of chromophores provided by the metal ions or ligand array in the cage superstructure, in close proximity to and surrounding a bound guest, generates a far higher local concentration of chromophores around the substrate than could be achieved simply by diffusion of separate chromophore and substrate units in solution. As such there has been considerable recent interest in development of strategies to incorporate photophysically active metal complex units or organic units into coordination cage superstructures.[4-10]

We reported recently how the octanuclear, approximately cubic coordination cage $[Cd_8(L^{napW})_{12}]^{16+}$, which is luminescent by virtue of the array of 12 naphthyl chromophores in the ligands around the cage periphery, could effect photoinduced electron transfer from a naphthyl group in its excited state to an electron-deficient guest such as 1,4-naphthoquinone (NQ) or 1,2,4,5-tetracyanobenzene (TCNB).[9] This coordination cage was an attractive target for this type of photophysical study on cage/guest complexes as it has exceptionally well-understood host-guest chemistry.[11-13] Binding of the guests in this cage cavity in water, which is driven by the hydrophobic effect,[12] resulted in quenching of the cage fluorescence and (in one case) the appearance of a detectable signal for a short-lived radical anion of the guest in UV/Vis transient absorption spectra, indicative of cage-to-guest photoinduced electron transfer which resulted in a short-lived $(naphthyl)^{\bullet+}/(TCNB)^{\bullet-}$ charge-separated state in the host/guest complex.[9]

More versatile photosensitisers to use in this context however are those based on phosphorescent complexes of d^6 transition metals such as Ru(II), Os(II) and Ir(III). These complexes have very well-established and beneficial photophysical properties, in terms of long-lived excited states which are able to participate in PET to or from a nearby quencher, and also the chemical stability of both redox partners; these desirable properties account for the extensive popularity of d^6

complexes in photo-redox catalysis.[14] Their kinetic inertness however makes self-assembly of coordination cages containing these units difficult. A common strategy to form a cage is therefore a stepwise one, in which a pre-formed metal complex fragment bearing pendant binding sites (a 'complex ligand') is combined with a labile ion in a second step, resulting in assembly of a heteronuclear cage which incorporates an array of phosphorescent metal complex units.[4b,8e,8f,10a] Using this strategy, we described recently the two-step formation of another member of our cubic cage family, $[Os_4Cd_4(L^{nap})_{12}](BF_4)_{16}$, in which four Os(II) complex units bound by three pyrazolyl-pyridine chelating ligands form four of the eight vertices of the cube, in a strictly alternating arrangement with the Cd(II) ions (Scheme 1).[10a] These Os(II) units were shown to have photophysical characteristics which are potentially useful for light-related applications, in particular a phosphorescent ^{3}MLCT excited state with a lifetime of hundreds of nanoseconds, and an excited-state oxidation potential which is sufficiently low to make them PET donors that are comparable to the well-known sensitiser $[Ru(bipy)_3]^{2+}$.[10a]

In this paper we report the preparation of the related photoactive cubic cage $[Os_4Zn_4(L^{nap})_{12}](ClO_4)_{16}$, its conversion to the water-soluble chloride salt (water-solubility is essential to allow strong binding of hydrophobic guests), and the photophysical consequences of binding a range of electron-deficient guests in the cage cavity in water. In particular we show by UV/Vis transient absorption spectroscopy that PET occurs from the array of Os(II) sensitisers in the cage array to the bound guest molecules, and describe the dynamic behaviour of the cage/guest assemblies in their excited states. The long-term goal is to use the cages as photo-redox catalysts, to effect catalytic transformations of bound guests: evaluating the ability of the cages to perform PET to bound guests, and characterising the nature and dynamic behaviour of the resulting charge-separated states, is the essential first step.

Results and Discussion

*Synthesis, characterisation and properties of the host cage **Os•Zn***

We have previously reported group of mixed-metal $[(M^a)_4(M^b)_4(L^{nap})_{12}]X_{16}$ cages, which contain Ru(II) and Os(II) metal centres as the four kinetically inert vertices (M^a).[10] These cages were prepared (Scheme 1) by initial formation of the mononuclear complex ligands $[M^a(L^{nap})_3]^{2+}$ in which the three ditopic ligands, L^{nap}, are coordinated to M^a *via* one terminus only, leaving three pendant binding sites at which the cage assembly could be propagated by reaction of four equivalents of $[M^a(L^{nap})_3]^{2+}$ with four equivalents of a labile metal ion M^b [Co(II) or Cd(II)]. Importantly, formation of the initial Ru(II) or Os(II) complexes $[M^a(L^{nap})_3]^{2+}$ with three pyrazolyl-pyridine chelates around each M^a centre occurs to give an approximately statistical *fac* : *mer* ratio of 1:3,[10] but these do not need separating for the next step as this family of octanuclear cubic cages contains two *fac* and six *mer* metal centres, so the 1:3 *fac*:*mer* ratio of $[M^a(L^{nap})_3]^{2+}$ metal complex units is precisely correct to be used for the final step to complete cage assembly.[15]

The new cage $[Os_4Zn_4(L^{nap})_{12}]Cl_{16}$ (abbreviated hereafter as **Os•Zn**) has two significant differences from the previously-reported heterometallic cubic cages.[10] Firstly, replacement of the traditional counter-ions (BF_4^-, PF_6^-; used to confer solubility in polar organic solvents) by chloride provides the necessary water-solubility that enables hydrophobic guests to bind.[16] Secondly, Cd(II) as the labile metal ion M^b has been replaced by Zn(II). In both cases the labile ion is d^{10} and therefore photophysically innocent, not causing any quenching of the excited state of the Os(II) vertices: however we found that, following conversion of the cages to the chloride form by ion-

exchange, the Os_4Zn_4 cage showed better long-term stability than the Os_4Cd_4 analogue, possibly because of the high affinity of chloride for Cd(II).

Os•Zn (as its perchlorate salt) was prepared by combination of $[Os(L^{nap})_3](PF_6)_2$ with excess $Zn(ClO_4)_2$ in nitromethane followed by slow crystallisation from nitromethane / diisopropyl ether to afford deep red X-ray quality crystals. The identity of the complex was confirmed by ES mass spectrometry, with the spectrum showing a characteristic sequence of signals $\{Os_4Zn_4(L^{nap})_{12}(ClO_4)_{16-n}\}^{n+}$ (n = 4, 5, 6) due to sequential loss of anions from the intact complex cage cation. The low symmetry of the complex (four independent ligands with no internal symmetry generates 88 independent proton environments, mostly in the aromatic region)[10] precludes assignment of the ^1H NMR spectrum, but a DOSY spectrum of the chloride salt (see SI, Fig. S1) showed that all signals had the same diffusion coefficient [log $D(m^2\ s^{-1})$ = –9.8] which is characteristic of an assembled cage and quite different from the less negative values associated with mononuclear complex fragments {*e.g.* log $D(m^2\ s^{-1})$ = –9.1 for $[Os(L^{nap})_3](PF_6)_2$}.[10]

The X-ray crystal structure (Fig. 1) shows that this cage has the same, approximately cubic, structure that we have observed for many other $[M_8(L^{nap})_{12}]X_{16}$ cages with other metal ions, with a metal ion at each vertex of the 8 vertices of the cube and a bridging ligand connecting two metal ions along every one of the 12 edges. This structural type has been described in detail before;[9-13] the key structural features such as the (non-crystallographic) S_6 symmetry arising from the arrangement of two *fac* and six *mer* tris-chelate sites (Scheme 1), the extensive inter-ligand π-stacking between electron-rich and electron-deficient fragments of different ligands around the periphery, and the presence of an anion in each of the portals on the centres of the six faces, are typical. The metal-metal separations along the edges of the cubic array of metal ions are 11.2 – 11.3 Å. In this structure, as in some of the previously-reported heterometallic cages $[(M^a)_4(M^b)_4(L^{nap})_{12}]X_{16}$ (M^a = Ru or Os, M^b = Co; M^a = Os, M^b = Cd),[10a] the two metal sites are indistinguishable crystallographically as the cage is disordered over two orientations such that each metal atom site is refined as a 50/50 mixture of Zn and Os.

To make the cage water-soluble, **Os•Zn** was converted from a perchlorate salt to a chloride salt, by stirring a suspension of $[Os_4Zn_4(L^{nap})_{12}](ClO_4)_{16}$ in water with an excess of Dowex ion-exchange resin to afford an aqueous solution of **Os•Zn** as the chloride salt. The electrochemical and photophysical properties of **Os•Zn** in water were investigated by UV/Vis absorption and luminescence spectroscopy, and cyclic voltammetry (Table 1; SI, Fig. S2). The properties of **Os•Zn** are virtually identical to those of the mononuclear component complex $[Os(L^{nap})_3]Cl_2$, with only small changes arising from assembly with Zn(II) ions to form the cage (*e.g.* the Os(II)/Os(III) redox potential for **Os•Zn** is 10 mV more positive than for mononuclear $[Os(L^{nap})_3]Cl_2$). The four Os(II)/Os(III) couples are coincident, with a single wave in the cyclic voltammogram that showed no signs of broadening or being split into four closely-spaced components, and fully chemically reversible. The chemical reversibility of the Os(II)/Os(III) redox process – *i.e.* the stability of both the Os(II) and Os(III) forms of the complex units – is an essential prerequisite for any possible use of **Os•Zn** to effect photo-redox catalysis on cavity-bound guests.

We also prepared the simpler mononuclear Os(II) model complex $[Os(L^{me})_3]Cl_2$ (Scheme 2) in order to be able to eliminate any substituent effects arising from the naphthyl units on the redox and luminescence properties of the Os(II) components in **Os•Zn**. Compared to both **Os•Zn** and $[Os(L^{nap})_3]Cl_2$, the Os(II)/Os(III) redox potential is *ca.* 100 mV less positive; and the emission maximum is slightly red-shifted to 655 nm. $[Os(L^{me})_3]Cl_2$, like $[Os(L^{nap})_3]Cl_2$, is also formed as a statistical mixture of *fac* and *mer* isomers (SI, Fig. S3). UV/Vis spectra are collected in Fig. 2. The

phosphorescence of the ^{3}MLCT state, for both mononuclear complexes $[Os(L^{nap})_3]Cl_2$ and $[Os(L^{me})_3]Cl_2$, decays with two distinct lifetime components with the ratio of the amplitudes (Fig. S4) corresponding approximately to the statistical 3:1 mixture of *mer:fac* isomers. In contrast, the luminescence decay of the assembled cage **Os•Zn** follows a mono-exponential decay (Table 1); using two components did not improve the quality of the fit. The time-resolved luminescence decay data with overlaid best fits are given in SI (Fig. S4).

It is clear from the data in Table 1 that the desirable photophysical properties of mononuclear $[Os(L^{nap})_3]Cl_2$, in particular the long-lived ^{3}MLCT excited state which is capable of acting as a good photo-electron donor,[10a] are preserved in the cage assembly **Os•Zn**. Importantly, no naphthalene-based emission was observed even when excitation was at 290 nm into the naphthalene-based absorption maximum of the **Os•Zn** cage, confirming that any ligand-based excited states that may be initially formed undergo fast intramolecular energy-transfer to the Os(II)-diimine units at the cage vertices from which the characteristic ^{3}MLCT phosphorescence occurs.

Guest binding

To explore the ability of the Os(II) chromophore in **Os•Zn** to act as an electron-donor from its ^{3}MLCT excited state, three electron-accepting guests (Scheme 3) have been studied which are all of an appropriate size to fit in the cage cavity and are sufficiently hydrophobic to ensure reasonable binding in water.[12c] Two of these guests (TCNB and NQ) were also shown in a recent study to bind in the cavity of the isostructural cage $[Cd_8(L^{napW})_{12}](NO_3)_{16}$, causing quenching of the naphthalene-based cage fluorescence.[9] 1-Nitronaphthalene (NN) has not been used as a guest before. All three guests (G) are sufficiently good electron acceptors to quench the Os-based MLCT excited state to give Os(III)/$G^{\bullet-}$ charge-separated states: the ^{3}MLCT excited-state energy of the Os units is 16,100 cm^{-1} (*ca.* 2 eV),[10a] and the potential required to oxidise Os(II) to Os(III) is *ca.* 0.7 V *vs.* SCE (Table 1), which means that any guest that can be reduced at a potential significantly less negative than –1.3 V *vs.* SCE should be able to quench the Os-based ^{3}MLCT excited state by PET.

Binding of these guests in the cavity of **Os•Zn** in water was examined by luminescence titrations. During addition of increasing amounts of guest to an aqueous solution of **Os•Zn**, the luminescence intensity steadily diminished as binding of the electron-accepting guest quenched the Os-based emission (Fig. 3a). In all cases the curve of emission intensity *vs.* guest concentration fitted well to a 1:1 binding isotherm (see inset to Fig. 3a), giving binding constants for all three guests in the range 10^3 M^{-1} – 10^4 M^{-1} (Table 2). The values obtained for NQ and TCNB are slightly smaller than were observed for binding in the cavity of $[Cd_8(L^{napW})_{12}](NO_3)_{16}$ (both > 10^4 M^{-1}),[9] which we ascribe to the presence of chloride as the counter-ion for **Os•Zn**; we have noticed before that use of chloride as counter-ions – excellent though it is for conferring water-solubility on the cages – reduces binding constants of guests, possibly due to competition from the chloride anion for guest binding in the cavity in aqueous solution.[16] Time-resolved measurements taken during the titrations of the guests into **Os•Zn** showed only a reduction in magnitude of the long-lived phosphorescence component as the amount of free cage decreased, with no short-lived emission components appearing associated with guest binding, which indicates that guest binding results in complete (within the sensitivity of our instruments) quenching of the Os-based emission from each cage.

Attempts to measure binding of these guests in the cavity of **Os•Zn** using ^{1}H NMR spectroscopy were unsuccessful due to substantial overlap of the ^{1}H NMR signals of the cage and the guests, and the presence of a large number of signals for the cage in a small chemical shift region which made it difficult to monitor small changes. However we could measure the binding constants

of these three guests in the cavity of the isostructural Co(II) cage $[Co_8(L^{nap})_{12}]Cl_{16}$,[16] by ^{1}H NMR titrations for comparison purposes: the paramagnetism of the high-spin Co(II) ions disperses the ^{1}H signals from the cage over a range of nearly 200 ppm, enabling the changes in cage ^{1}H signals associated with guest binding to be detected easily and used to calculate binding constants (Fig. 3b).[12a,12b] The values of the binding constants obtained from ^{1}H NMR titrations of the three guests in $[Co_8(L^{nap})_{12}]Cl_{16}$ (Table 2) are reassuringly comparable to the values obtained by luminescence quenching of isostructural **Os•Zn** by the same guests. At the end of these titrations we could observe new signals in the ^{1}H NMR spectra for these cage/guest assemblies in the region –1 to –5 ppm (SI, Fig. S5), associated with a guest being bound inside a cavity in slow exchange on the NMR timescale, surrounded by eight paramagnetic ions which cause the substantial change in the guest's chemical shift. We have previously confirmed that new signals in this region of the NMR spectrum when cage/guest complexes form are associated specifically with bound guests.[13]

Guest binding inside the cage cavity was finally confirmed by the crystal structure of the cage/guest adduct using $[Co_8(L^{nap})_{12}](BF_4)_{16}$ which provides a cage environment isostructural with that of **Os•Zn.** The adduct of $[Co_8(L^{nap})_{12}](BF_4)_{16}$ with TCNB was prepared using the same 'crystalline sponge' method – treating pre-formed crystals of the empty host $[Co_8(L^{nap})_{12}](BF_4)_{16}$ with a concentrated solution of the guest in MeOH – that we have successfully used before to prepare X-ray quality crystals of cage/guest complexes with this system.[6,11,12b] Fig. 4a shows the crystal structure of this cage/guest assembly in which one molecule of TCNB is centrally positioned in the cage cavity, astride the inversion centre, with an opposed pair of cyano groups directed into the two H-bond donor pockets associated with the two *fac* tris-chelate metal vertices located at either end of the long diagonal of the cage (Fig. 4b). This allows the lone pairs on each of those two N atoms to participate in a network of weak CH•••N interactions with a set of convergent CH protons that lie close to the cationic metal centres, which collectively form an H-bond donor site comparable in strength to phenol.[13a] These CH•••N interactions – principally involving atom N(15G) but also involving atom N(17G – result in non-bonded C•••N separations in the range 3.38 – 3.40 Å, with the CN•••HC distances in the range 2.48 – 2.75 Å.

The position of the nitrile N atom – N(15G) and its symmetry equivalent – in this H-bonding pocket results in an N(15G)•••Co(4) separation of 5.33 Å, comparable to what we observe with a range of other guests whose electron-rich regions occupy this hydrogen-bond donor pocket. This type of H-bonding interaction occurs in all cage/guest complexes that we have structurally characterised and anchors the guests in place.[11,15] What is interesting here is that the dimensions of TCNB are fortuitously ideal to allow the guest to span the cavity and be anchored at both ends, suggesting interesting possibilities for future work on guest binding based on multiple H-bonding interactions.

Transient absorption studies.

The excited-state behaviour of the **Os•Zn** cage and its cage/guest assemblies were investigated using ultrafast UV/Vis transient absorption (TA) spectroscopy, with the aim to detect differences between the excited state behaviour of **Os•Zn** in the absence and presence of a guest. The TA spectra were recorded in aqueous solutions, using excitation with ~40 fs pulses at 400 nm [into the ^{1}MLCT absorption manifold associated with the Os(II) units]. The TA spectrum of mononuclear $[Os(L^{me})_3]Cl_2$ (Scheme 2) – prepared as a model for the Os(II) units in the cage, and isolated as a 1:3 statistical mixture of *fac* and *mer* isomers,[15] reflecting the proportions in the **Os•Zn** cage – immediately after excitation shows bleaches at 425 and across the 520-560 nm region

relating to loss of the ground-state absorption – exactly mirroring the shape of the UV/Vis absorption spectrum in this region (Fig. 5a). The bleaching of the ground state is accompanied by formation of new transient absorption bands at around 610 and 350 nm. The new absorption band at 610 nm is assigned to transient oxidation of the Os(II) vertex to Os(III) in the MLCT excited state: previous spectro-electrochemical studies confirm that the broad region of absorption between 600 and 700 nm is associated with formation of Os(III) vertices (see SI, Fig. S6).[10a] The increased absorption at *ca.* 350 nm can reasonably be assigned to the $(pypz)^{\bullet-}$ radical anion that is also formed in the ^{3}MLCT excited state; we do not have confirmation of this assignment by spectro-electrochemistry as the ligand-based reductions of these pypz complexes are irreversible, but changes in the π-π* absorption manifold associated with ligands in the UV region are to be expected when a ligand is transiently reduced to its radical anion.

These transient features in the absorption spectrum of $[Os(L^{me})_3]Cl_2$ decay synchronously with the bleach recovery. The transient spectrum does not decay completely by the instrument-determined limit of 7.5 ns, suggesting the presence of a much longer-lived decay component (in agreement with the luminescence measurements, Table 1). The kinetic data were modelled using global analysis in a 4-component model where the two long lifetimes (206 and 97 ns) were fixed to match the luminescence decay data, and additional fast processes with time constants of 1.6 ps (likely vibrational cooling)[17] and 140 ps were identified (the latter, low-amplitude, component is too slow for vibrational cooling, and implies a more substantial structural rearrangement, perhaps associated with a distortion of the metal coordination sphere in the excited state). Overall the transient absorption spectra and dynamic behaviour observed for $[Os(L^{me})_3]Cl_2$ are consistent with typical formation and decay of a ^{3}MLCT state.

The assembled cage **Os•Zn** demonstrated transient absorption behaviour (Fig. 5b) which was very similar to that of the monomer, confirming what was apparent from the redox and luminescence data, *viz.* that coordination of the pendant pyrazolyl-pyridine units of $[Os(L^{nap})_3]Cl_2$ to Zn(II) ions to complete the cage assembly has very little effect on the properties of the Os(II) units. Again we observe, following 400 nm / 40 fs pulse excitation, bleaches of the UV/Vis absorption bands associated with the ^{1}MLCT absorptions and appearance of new transient signals associated with formation of a ^{3}MLCT state (Fig. 5b) as described above for $[Os(L^{me})_3]Cl_2$.

The transient features in the absorption spectrum of **Os•Zn** decay synchronously with the bleach recovery. The kinetic data modelled using global analysis, with a fixed time constant of >50 ns (to match luminescence data, although on the time scale of the experiment, this lifetime can be considered as a constant background level), revealed two fast processes with the time constants of sub-ps (likely due to vibrational cooling)[17] and ~1 ns, most likely due to a distortion of the metal coordination sphere in the excited state which occurs on a somewhat longer time scale than in the mononuclear complex due to the rigidity of the cage. Decay-associated spectra obtained by global analysis of the TA data (sequential model), corresponding to the species decaying with each of the different time constants, are shown in Fig. S7.

The TA experiments were then conducted on solutions of **Os•Zn** cage (0.15 mM) in the presence of a sufficient excess of guest (0.4 - 1.5 mM) to ensure that a substantial proportion (>70 %) of the cage contained bound guest, based on the binding constants in Table 2. Any differences in the transient absorption spectral features, and kinetic behaviour between free **Os•Zn** and the **Os•Zn**/guest assemblies, will be indicative of photoinduced electron transfer between cage and guest. The results of the global analyses of the TA data for each cage/guest assembly (see SI for details, Figs. S8 - S11) are summarised in Table 2. In each case, in the presence of the guest, we

require two additional kinetic components in order to satisfactorily fit the data using global analysis. The shorter of these (timescale 13 – 21 ps) is associated with the grow-in of new features in the TA spectrum and can therefore be tentatively ascribed to a forward PET process, from the ^{3}MLCT excited state of one of the Os(II) units in the cage to the bound guest, generating an Os^{3+}/guest$^{\bullet-}$ charge-separated state. When TCNB is used as the guest, the grow-in of this charge-separated state is particularly prominent due to the narrow and intense absorption feature of its radical anion at 460 nm; the grow-in for the radical anions of the other two guests is less pronounced in the TA data, but is nonetheless clearly evident in the global analysis. The second additional kinetic component is for the decay of the features associated with this excited state, with a lifetime of *ca.* 200 ps in every case: this is consistent with "geminate recombination" of the short-lived charge-separated state which has formed following PET. The time constants of this new decay process (Table 2) are similar for all three **Os•Zn**/guest combinations, within 1 standard deviation of each other. We note that decay of the (napthyl)$^{\bullet+}$/(TCNB)$^{\bullet-}$ charge-separated state based on $[Cd_8(L^{napW})_{12}](NO_3)_{16}$ as host and TCNB as guest occurred on broadly comparable timescales with decay components of 32(±11) and 1130(±150) ps.[9]

Further analysis of the TA data was performed on each of the **Os•Zn**/guest assemblies through spectral subtractions, to reveal the transient spectral features associated only with these short-lived charge-separated states in the cage/guest structures; this was performed by subtraction of the longest time delay spectrum (5 ns after excitation) from a series of spectra obtained after shorter time delays from 5 ps - 1 ns. This subtraction was necessary to account for the transient absorption signals arising from *ca.* 30% of the unoccupied cage present in the equilibrium mixture. The resulting spectra (Fig. 6) reveal new transient absorption features which are associated with the two short-lived kinetic components (grow-in and decay), and which match those of the guest radical anions, by comparison with the published spectra of TCNB$^{\bullet-}$ (maximum at 462 nm),[18] NQ$^{\bullet-}$ (maximum at 550 nm),[19] and NN$^{\bullet-}$ (maximum at 465 nm; recorded in this work in a spectro-electrochemical experiment, see SI, Fig. S12). The main absorption spectral features associated with these radical anions are collected in Table 2. The broad transient feature in the 600 – 700 nm region in all three transient spectra is associated with the Os(III) centre of the ^{3}MLCT excited state, as mentioned earlier (SI, Fig. S6).

Decay-associated spectra obtained from the global analysis of the **Os•Zn**/TCNB system are shown in Fig. 7a for two of the lifetime components: the brown spectrum is associated with the long-lived component (empty **Os•Zn** cage present in the equilibrium, >50 ns) and the red spectrum is associated with the short-lived component from the **Os•Zn**/TCNB charge-separated excited state (*ca.* 200 ps). The transient absorption spectral features of the cage are present in both spectra, however when these spectra are subtracted from one another to remove the long-lived contribution from empty **Os•Zn** cage, the spectrum in Fig. 7b (purple) is obtained which corresponds to the Os^{3+}/TCNB$^{\bullet-}$ charge-separated component alone, and matches well with the combined absorption spectra of the (TCNB)$^{\bullet-}$ anion (460 nm, sharp feature) and the Os^{3+} unit (broad absorption around 650 nm). Thus the short-lived (*ca.* 200 ps) species is indeed the charge-separated Os^{3+}/TCNB$^{\bullet-}$ state arising from PET in the cage/guest assembly. Similar analyses are also shown in Fig. 7b and S8, providing comparable confirmation of the nature of the transient species for the **Os•Zn** complexes with NQ and NN (NQ: 550 nm, broad absorption; NN: 465 nm, sharp absorption). Detailed kinetic analyses are given in the SI (Fig. S10 and S11).

Finally, we needed to confirm that this PET process is happening within the cage cavity, and is not just associated with interaction of the guest with the external surface of the cage or simply by

collision between chromophore and quencher in solution without guest binding in the cage cavity. Two types of control experiments have been performed. Firstly, we added to each **Os•Zn**/guest complex an excess of cycloundecanone, a competing guest that binds much more strongly in the cage cavity than TCNB, NQ or NN,[12b] but is photophysically innocent. This resulted (Fig. 8) in loss of the short-lived grow-in and decay components associated with the cage/guest charge-separated state, and restoration of the long-lived decay associated with the empty cage – or, in this case, the cage occupied by an inert guest that has no effect on the excited-state behaviour. Thus, having confirmed from the decay-associated spectra that the *ca.* 200 ps component in each case is associated with a charge-separated state generated by cage-to-guest PET, we have also confirmed that this is associated with the guest being inside the cage cavity and does not form when the guest is displaced.

Secondly, we compared the TA experiments on the **Os•Zn**/TCNB adduct (which shows the presence of the transient signal associated with formation of the $TCNB^{\bullet-}$ radical anion: see Fig. 6, top panel) with the results of an identical TA experiment in which the cage **Os•Zn** was replaced by four equivalents of $[Os(L^{me})_3]Cl_2$ to give the same number of Os(II) chromophores, with the same optical density at the excitation wavelength, in the solution. In this experiment (SI, Fig. S11) there is no detectable absorption feature associated with formation of $TCNB^{\bullet-}$, confirming that it is not just the presence of the Os(II) chromophores that is essential for the PET to occur, but their assembly into a cage which can bind the guests in its central cavity.

Conclusion

In conclusion, we have prepared a water-soluble octanuclear cubic host cage **Os•Zn**, which contains $[Os(pyrazolyl\text{-}pyridine)_3]^{2+}$ units at four of the eight vertices, by a stepwise 'complexes as ligands' strategy. These Os(II) complex units have a long-lived ^{3}MLCT excited state which is a good photo-electron donor and is capable of effecting photoinduced electron-transfer (timescale 10 – 20 ps) to any of three different electron-deficient aromatic guests which bind in the cage cavity, giving in each case a $cage^{\bullet+}/guest^{\bullet-}$ charge-separated state with a lifetime of *ca.* 200 ps. Transient absorption spectra clearly identified spectral features associated with the guest radical anion in each case, specifically associated with the short-lived charge-separated species; and addition of a competing (photophysically innocent) guest removed the short-lived spectral features associated with formation $cage^{\bullet+}/guest^{\bullet-}$ confirming that this requires the guest to be cavity-bound. The ability of these photo-active cages to both bind a guest in a cavity surrounded by multiple luminophores, and then to be involved in photophysical processes with bound guests, offers interesting possibilities in areas such as photo-redox catalysis[14] of bound guests, and even multiple accumulative electron transfer from two or more strongly electron-donating chromophores to a single electron-deficient bound guest[20] if the redox potentials are appropriate and the guest is trapped in the cavity for long enough. Such studies are in progress.

Experimental

$[Co_8(L^{nap})_{12})]Cl_{16}$ (used for the ^{1}H NMR titrations),[16] 3-(2-pyridyl)pyrazole,[21] and $[Os(L^{nap})_3](PF_6)_2$ (mix of *fac* and *mer* isomers)[10a] were prepared as reported previously. Single crystals of $[Co_8(L^{nap})_{12})](BF_4)_{16}$ used for determination of the structure of the $[Co_8(L^{nap})_{12})](BF_4)_{16}$•TCNB adduct were also prepared as described previously.[12b]. The three guests and other organic reagents / metal salts were purchased from Alfa or Sigma-Aldrich and used as received. Instruments used for routine

NMR spectroscopic and mass spectrometric measurements have been reported in a previous publication.[10a]. Details of X-ray crystallographic measurements are given in SI.

^{1}H NMR titrations to evaluate guest binding in the cavity of $[Co_8(L^{nap})_{12})]Cl_{16}$ in D_2O were performed as previously reported.[22] All binding experiments were performed in triplicate; the values for binding constants quoted are the average of the three measurements rounded to 1 significant figure. For the fast exchange cases, the changes in chemical shift were plotted and fitted to a 1:1 host:guest binding model. For the slow exchange cases, where separate sets of signals for free cage and cage/guest peaks are observed, binding constants were determined by deconvolution and integration of the signals.

Luminescence titrations were performed by preparing a stock solution of $[Os_4Zn_4(L^{nap})_{12}]Cl_{16}$ (0.025 mM) in deionised water. Guest solutions (0.5 - 3 mM) were made up using this stock host solution (5 ml) and added in small portions to the quartz cuvette containing the host solution, with a luminescence spectrum measured after each addition. Luminescence spectra were recorded on a Horiba Jobin Yvon Fluoromax 4 spectrophotometer, with excitation at 550 nm and an emission window of 570 – 850 nm. Changes in luminescence intensity with added guest concentration were fitted to a 1:1 host:guest binding model. Luminescence lifetimes were measured using an Edinburgh Instruments 'Mini-τ' instrument, using a 405 nm, ~75 ps pulsed diode laser excitation source, with lifetimes calculated using the supplied software.

Cyclic voltammetry was performed in water using 0.1M NaCl as base electrolyte. The potential was controlled with an Emstat^{3+} Potentiostat using PSTrace software. A solvent-saturated atmosphere of nitrogen was used to degas the sample and all measurements were performed under an inert atmosphere of nitrogen. The electrodes used were a glassy carbon working electrode, a platinum strip counter electrode and an Ag/AgCl reference electrode. All potentials are quoted versus SCE; scan rates used were 10 – 100 mV s^{-1}.

UV/Vis Spectroelectrochemical measurements were performed, in dry acetonitrile at 253K on a Cary 5000 spectrophotometer using a home-built OTTLE cell as previously reported,[23] with a Pt mesh working electrode, a Pt wire counter electrode and Ag wire pseudo-reference electrode.

Transient absorption spectroscopy. The ultrafast transient absorption setup used consists of a commercial detection instrument (Helios, Ultrafast Systems) and the following laser system: a Ti:Sapphire regenerative amplifier (Spitfire ACE PA-40, Spectra-Physics) providing 800 nm pulses (40 fs fwhm, 10 kHz, 1.2mJ). Sample excitation was provided by doubling a portion of the 800 nm output, in a β-barium borate crystal within a commercially available doubler/tripler (TimePlate, Photop Technologies), yielding 400 nm pulses. White light supercontinuum probe pulses were generated *in situ* using a portion of the Ti:Sapphire amplifier output, focused onto a CaF_2 crystal, allowing for the generation of light spanning 340 nm – 720 nm. Detection was performed with a CMOS sensor for UV/Vis spectra. The pump and probe polarisations were set to a magic angle geometry. The data processing was performed using Origin 2017[24] and Glotaran 1.5.1.[25]

Synthesis of $[Os_4Zn_4(L^{nap})_{12}](ClO_4)_{16}$. **CAUTION: Perchlorate salts are potentially explosive and should be handled with care and only in small quantities.** $[Os(L^{nap})_3](PF_6)_2$ (0.032 g, 0.018 mmol) and $Zn(ClO_4)_2{\cdot}6H_2O$ (0.067 g, 0.18 mmol) were stirred in nitromethane (15 ml) overnight. The

mixture was filtered and then crystallised by slow diffusion of di-isopropyl ether into the $MeNO_2$ solution. The pure crystalline product was collected by filtration and washed with di-isopropyl ether, methanol, and diethyl ether. Yield: 0.050 g, 0.005 mmol, 21%. ESMS: *m/z* 1220.4 $(M - 6ClO_4)^{6+}$; 1482.2 $(M - 5ClO_4)^{5+}$; 1881.3 $(M - 4ClO_4)^{4+}$ (most intense component of isotope cluster given in each case). UV/Vis in MeCN [λ_{max}/nm (10^{-3} ε/M^{-1} cm^{-1})]: 555 (sh), 510 (sh), 426 (48), 400 (sh), 287 (310), 227 (560). For conversion to the water-soluble chloride salt **Os•Zn**, $[Os_4Zn_4(L^{nap})_{12}](ClO_4)_{16}$ (26 mg, 0.004 mmol) was mixed with 1x2 Dowex, in distilled water (15 ml) and left to stir at room temperature for 4 hours, until the complex had completely dissolved. The sample was filtered through a microporous filter before use. Crystallographic details for the structure determination of $[Os_4Zn_4(L^{nap})_{12}](ClO_4)_{16}$ are in the Supporting Information.

Synthesis of $[Os(L^{H})_3](PF_6)_2$ *(mixture of fac and mer isomers).* 3-(2-Pyridyl)pyrazole (0.166 g, 1.14 mmol), $OsCl_3.6H_2O$ (0.106 g, 0.30 mmol) and ethylene glycol (7 ml) were combined in a 10 ml microwave tube, which was then heated in a microwave synthesiser (Discovery S, CEM Microwave Technology) to 200 °C for 3h. The solution was allowed to cool and an aqueous solution of KPF_6 (30 ml) was added. The resulting suspension was then filtered over celite to yield a brown precipitate and a red solution. The solution was then extracted with several portions of DCM and the solvent was removed *in vacuo*. The resultant precipitate was next purified using column chromatography on silica by elution with MeCN/water/saturated aqueous KNO_3 (100:5:1, *v/v/v*) and the first red band was collected and the solvent removed *in vacuo*. The product was dissolved in water, and aqueous KPF_6 and DCM were added to perform a solvent extraction of the hexafluorophosphate salt of the complex into DCM. The solvent was removed by evaporation and the pure product was then dried *in vacuo*. Yield: 0.185 g, 0.20 mmol, 67 %. The ^{1}H NMR spectrum is broadened by hydrogen-bonding aggregation in solution, but the number of signals is consistent with the 1:3 ratio of *fac:mer* isomers which results in four distinct ligand environments with equal likelihood.[15] ^{1}H NMR (400 MHz, CD_3CN): δ 8.12 (m, 4H), 7.75 (m, 4H), 7.72 (m, 4H), 7.59 – 7.50 (m, 2H), 7.42 (m, 2H), 7.21 – 7.04 (m, 8H). ESMS: *m/z* 626.1 $(M - 2PF_6 - H^+)^{1+}$, 313.6 $(M - 2PF_6)^{2+}$.

Synthesis of $[Os(L^{me})_3](PF_6)_2$. $[Os(L^{H})_3](PF_6)_2$ (0.185 g, 0.2 mmol) was dissolved in MeCN (50 ml), to which Cs_2CO_3 (0.470 g, 1.4 mmol) and methyl iodide (0.67 ml, 10.8 mmol) were added and the solution was left to reflux for 18 hours. The mixture was left to cool, excess Cs_2CO_3 was filtered off, and then the solvent was removed *in vacuo*. The resultant precipitate was then purified using column chromatography on silica by elution with MeCN/water/saturated aqueous KNO_3 (100:10:2, *v/v/v*). The main red band was collected and dissolved in water; addition of aqueous KPF_6 and DCM allowed solvent extraction of the hexafluorophosphate salt into DCM to be performed. Evaporation of the solvent afforded a pure red precipitate. Yield: 0.184 g, 0.19 mmol, 96 %. ^{1}H NMR (400 MHz, CD_3CN): δ 8.14 (m, 4H), 7.86 – 7.70 (m, 4H), 7.68 (m, 4H), 7.66 (d, 1H), 7.57 (d, 1H), 7.36 (d, 1H), 7.31 (d, 1H), 7.24 – 7.10 (m, 8H), 3.21 (s, 3H), 3.16 (s, 3H), 3.11 (s, 3H), 3.06 (s, 3H) ESMS: *m/z* 334.6 $(M - 2PF_6)^{2+}$. $[Os(L^{me})_3](PF_6)_2$ could be converted to its water-soluble chloride salt by ion-exchange with Dowex 1x2 resin, as described above for the **Os•Zn** cage.

Acknowledgements

We thank EPSRC for a PhD studentship (JST); research grant EP/N031555 (post-doctoral fellowship to AJM and CGPT); the EPSRC Capital Equipment award for the laser laboratory in Sheffield

(EP/L022613/1); the Leverhulme Trust for research grant RPG-2013-308 (post-doctoral fellowship to ABW), and the Universities of Warwick and Sheffield for support. We acknowledge the Diamond Light Source for time on beamline I-19 under proposal MT19876, and thank in particular Dr. Sarah Barnett for her assistance. Dr. Jerico Piper and Miss Cristina Mozaceanu are thanked for their help with the crystallographic data collection for $[Co_8(L^{nap})_{12}](BF_4)_{16}\bullet$ 0.66(TCNB).

Supporting Information

The Supporting Information is available free of charge on the ACS publication website at…

• Additional figures relating to characterization and photophysical analysis of the complexes: DOSY and ^{1}H NMR spectra; cyclic voltammograms; UV/Vis spectra; phosphorescence decay traces for the Os(II) complexes with fits to calculated lifetimes, and residuals; ^{1}H NMR spectra in the 0 to –14 ppm region of the Co_8 cage / guest complexes, showing signals associated with bound guests; decay-associated spectra for **Os•Zn** cage/guest complexes from TA data; spectroelectrochemistry of NN; results of TA control experiments; summary of X-ray crystallographic data for the two structures.

References

1 Reviews: (a) Chakrabarty, R. J.; Mukherjee, P. S.; Stang, P. J. Supramolecular Coordination: Self-Assembly of Finite Two- and Three-Dimensional Ensembles. *Chem. Rev.* **2011**, *111*, 6810. (b) Zhang, Y.-Y.; Gao, W.-X.; Lin, L.; Jin, G.-X. Recent advances in the construction and applications of heterometallic macrocycles and cages. *Coord. Chem. Rev.* **2017**, *344*, 323. (c) Cook, T. R.; Zheng, Y.-R.; Stang, P. J. Metal–Organic Frameworks and Self-Assembled Supramolecular Coordination Complexes: Comparing and Contrasting the Design, Synthesis, and Functionality of Metal-Organic Materials. *Chem. Rev.* **2013**, *113*, 734. (d) Pluth, M. D.; Bergman, R. G.; Raymond, K. N. Proton-Mediated Chemistry and Catalysis in a Self-Assembled Supramolecular Host. *Acc. Chem. Res.* **2009**, *42*, 1650. (e) Smulders, M. M. J.; Riddell, I. A.; Browne, C.; Nitschke, J. R. Building on Architectural Principles for Three-Dimensional Metallosupramolecular Construction. *Chem. Soc. Rev.* **2013**, *42*, 1728. (f) Zarra, S.; Wood, D. M.; Roberts, D. A.; Nitschke, J. R. Molecular Containers in Complex Chemical Systems. *Chem. Soc. Rev.* **2015**, *44*, 419. (g) Vardhan, H.; Yusubov, M.; Verpoort, F. Self-Assembled Metal-Organic Polyhedra: An Overview of Various Applications. *Coord. Chem. Rev.* **2016**, *306*, 171. (h) Schmidt, A.; Casini, A.; Kuhn, F. E. Self-Assembled M_2L_4 Coordination Cages: Synthesis and Potential Applications. *Coord. Chem. Rev.* **2014**, *275*, 19. (i) Custelcean, R. Anion Encapsulation and Dynamics in Self-Assembled Coordination Cages. *Chem. Soc. Rev.* **2014**, *43*, 1813. (j) Han, M.; Engelhard, D. M.; Clever, G. H. Self-Assembled Coordination Cages Based on Banana-Shaped Ligands. *Chem. Soc. Rev.* **2014**, *43*, 1848. (k) Amouri, H.; Desmarets, C.; Moussa, J. Confined Nanospaces in Metallocages: Guest Molecules, Weakly Encapsulated Anions, and Catalyst Sequestration. *Chem. Rev.* **2012**, *112*, 2015. (l) Yoshizawa, M.; Yamashina, M. Coordination-driven Nanostructures with Polyaromatic Shells. *Chem. Lett.* **2017**, *46*, 163. (m) Ward, M. D.; Hunter, C. A.; Williams, N. H. Guest Binding and Catalysis in the Cavity of a Cubic Coordination Cage. *Chem. Lett.* **2017**, *46*, 2. (n) Ahmad, N.; Younus, H. A.; Chugtai, A. H.; Verpoort, F. Metal-Organic Molecular Cages: Applications of Biochemical Implications. *Chem. Soc. Rev.* **2015**, *44*, 9.

2 Brown, C. J.; Toste, F. D.; Bergman, R. G.; Raymond, K. N. Supramolecular Catalysis in Metal-Ligand Cluster Hosts. *Chem. Rev.* **2015**, *9*, 3012.

3 (a) Therrien, B. Transporting and Shielding Photosensitisers by Using Water-Soluble Organometallic Cages: A New Strategy in Drug Delivery and Photodynamic Therapy. *Chem. Eur. J.* **2013**, *19*, 8378. (b) Therrien, B. Drug Delivery by Water-Soluble Organometallic Cages. *Top. Curr. Chem.* **2012**, *319*, 35.

4 (a) Ward, M. D. Photophysical Properties of Coordination Cages and Their Host/Guest Assemblies. In: Atwood, J. L., (ed), *Comprehensive Supramolecular Chemistry II,* **2017**, *6*, 357 (Elsevier, Oxford). (b) Luis, E. T.; Iranmanesh, H.; Arachchige, K. S. A.; Donald, W. A.; Quach, G.; Moore, E. G.; Beves, J. E. Luminescent Tetrahedral Molecular Cages Containing Ruthenium(II) Chromophores. *Inorg. Chem.* **2018**, *57*, 8476. (c) Li, X.-Z.; Zhou, L.-P.; Yan, L.-L.; Yuan, D.-Q. Lin, C.-S.; Sun, Q.-F. Evolution of Luminescent Supramolecular Lanthanide $M_{2n}L_{3n}$ Complexes from Helicates and Tetrahedra to Cubes. *J. Am. Chem. Soc.* **2017**, *139*, 8237. (d) Saha, M. L.; Yan, X.-Z.; Stang, P. J. Photophysical Properties of Organoplatinum(II) Compounds and Derived Self-Assembled Metallacycles and Metallacages: Fluorescence and its Applications. *Acc. Chem. Res.* **2016**, *49*, 2527.

5 (a) Shanmugaraju, S.; Mukherjee, P. S. Self-assembled discrete molecules for sensing nitroaromatics. *Chem. Eur. J.* **2015**, *21*, 6656. (b) Yin, S.-Y.; Zhu, Y.-X.; Pan, M.; Wei, Z.-W.; Wang, H.-P.; Fan, Y.-N.; Su, C.-Y. Nanosized NIR-Luminescent Ln Metal-Organic Cage for Picric Acid Sensing. *Eur. J. Inorg. Chem.* **2017**, 646. (c) Yan, X; Wang, H.; Hauke, C. E.; Cook, T. R.; Wang, M.; Saha, M. L.; Zhou, Z.; Zhang, M; Li, X.; Huang, F.; Stang, P. J. A Suite of Tetraphenylethylene-Based Discrete Organoplatinum(II) Metallacycles: Controllable Structure and Stoichiometry, Aggregation-Induced Emission, and Nitroaromatics Sensing. *J. Am. Chem. Soc.* **2015**, *137*, 15276.

6 Taylor, C. G. P.; Piper, J. R.; Ward, M. D. Binding of Chemical Warfare Agent Simulants as Guests in a Coordination Cage; Contributions to Binding and a Fluorescence-Based Response. *Chem. Commun.* **2016**, *52*, 6225.

7 (a) Liu, Y.; Wu, X.; He, C.; Li, Z.; Duan, C. Metal-Organic Polyhedra for Selective Sensing of Ribonucleosides Through the Cooperation of Hydrogen-Bonding Interactions. *Dalton Trans.* **2010**, *39*, 7727. (b) Zhao, L.; Qu, S.; He, C.; Zhang, R.; Duan, C. Face-driven octanuclear cerium(IV) luminescence polyhedra: synthesis and luminescent sensing natural saccharides. *Chem. Commun.* **2011**, *47*, 9387.

8 (a) Dalton, D. M.; Ellis, S. R.; Nichols, E. M.; Mathies, R. A.; Toste, F. D.; Bergman, R. G.; Raymond, K. N. Supramolecular $[Ga_4L_6]^{12-}$ Cage Photosensitises 1,3-Rearrangement of Encapsulated Guest *via* Photoinduced Electron Transfer. *J. Am. Chem. Soc.* **2015**, *137*, 10128. (b) Furutani, Y.; Kandori, H.; Kawano, M.; Nakabayashi, K.; Yoshizawa, M.; Fujita, M. *In Situ* Spectroscopic, Electrochemical, and Theoretical Studies of the Photoinduced Host-Guest Electron Transfer That Precedes Unusual Host-Mediated Alkane Photooxidation. *J. Am. Chem. Soc.* **2009**, *131*, 4764. (c) Jing, X.; He, C.; Yang, Y.; Duan, C. A Metal-Organic Tetrahedron as a Redox Vehicle to Encapsulate Organic Dyes for Photocatalytic Proton Reduction. *J. Am. Chem. Soc.* **2015**, *137*, 3967. (d) Martir, D. R.; Pizzolante, A.; Escudero, D.; Jacquemin, D.; Warriner, S. L.; Zysman-Colman, E. Photoinduced Energy and Electron Transfer Between a Photoactive Cage Based on a Thermally Activated Delayed Fluorescence Ligand and Encapsulated Fluorescent Dyes. *ACS Appl. Energy. Mater.* **2018**, *1*, 2971. (e) Guo, J.; Xu, Y.-W.; Li, K.; Xiao, L.-M.; Chen, S.; Wu, K.; Chen, X.-D.; Fan, Y.-Z.; Liu, J.-M.; Su, C.-Y. Regio- and Enantioselective Photodimerization Within the Confined Space of a Homochiral Ruthenium/Palladium Heterometallic Coordination Cage. *Angew. Chem. Int. Ed.* **2017**, *56*, 3852. (f) Chen, S.; Li, K.; Zhao, F.; Zhang, L.; Pan, M.; Fan, Y.-Z.; Guo, J.; Shi, J.; Su, C.-Y. A Metal-Organic Cage Incorporating Multiple Light Harvesting and Catalytic Centres for Photochemical Hydrogen Production. *Nat. Comm.* **2016**, *7*, 13169. (g) Yang, L.; He, C.; Liu, X.; Zhang, J.; Sun, H.; Guo, H. Supramolecular Photoinduced Electron Transfer Between a Redox-Active Hexanuclear Metal-Organic Cylinder and an Encapsulated Ruthenium(II) Complex. *Chem. Eur. J.* **2016**, *22*, 5253.

9 Piper, J. R.; Cletheroe, L.; Taylor, C. G. P.; Metherell, A. J.; Weinstein, J. A.; Sazanovich, I. V.; Ward, M. D. Photoinduced Energy- and Electron-Transfer From a Photoactive Coordination Cage to Bound Guests. *Chem. Commun.* **2017**, *53*, 408.

10 (a) Wragg, A. B.; Metherell, A. J.; Cullen, W.; Ward, M. D. Stepwise Assembly of Mixed-Metal Coordination Cages Containing Both Kinetically Inert and Kinetically Labile Metal Ions: Introduction of Metal-Centred Redox and Photophysical Activity at Specific Sites. *Dalton Trans.* **2015**, *44*, 17939. (b) Metherell, A. J.; Ward, M. D. Stepwise Synthesis of a Ru_4Cd_4 Coordination

Cage Using Inert and Labile Subcomponents: Introduction of Redox Activity at Specific Sites. *Chem. Commun.* **2014**, *50*, 6330.

11 Ward, M. D.; Hunter, C. A.; Williams, N. H. Coordination Cages Based on Bis(pyrazolylpyridine) Ligands: Structures, Dynamic Behavior, Guest Binding and Catalysis. *Acc. Chem. Res.* **2018**, in press (DOI: 10.1021/acs.accounts.8b00261)

12 (a) Whitehead, M.; Turega, S.; Stephenson, A.; Hunter, C. A.; Ward, M. D. Quantification of Solvent Effects on Molecular Recognition in Polyhedral Coordination Cage Hosts. *Chem. Sci.* **2013**, *4*, 2744. (b) Turega, S.; Cullen, W.; Whitehead, M.; Hunter, C. A.; Ward, M. D. Mapping the Internal Recognition Surface of an Octanuclear Coordination Cage Using Guest Libraries. *J. Am. Chem. Soc.* **2014**, *136*, 8475. (c) Cullen, W.; Turega, S.; Hunter, C. A.; Ward, M. D. Virtual Screening for High Affinity Guests for Synthetic Supramolecular Receptors. *Chem. Sci.* **2015**, *6*, 2790.

13 (a) Turega, S.; Whitehead, M.; Hall, B. R.; Meijer, A. J. H. M.; Hunter, C. A.; Ward, M. D. Shape-, Size- and Functional Group-Selective Binding of Small Organic Guests in a Paramagnetic Coordination Cage. *Inorg. Chem.* **2013**, *52*, 1122. (b) Cullen, W.; Thomas, K. A.; Hunter, C. A.; Ward, M. D. pH-Controlled selection between one of three guests from a mixture using a coordination cage host. *Chem. Sci.* **2015**, *6*, 4025.

14 (a) Staveness, D.; Bosque, I.; Stephenson, C. R. J. Free Radical Chemistry Enabled by Visible Light-Induced Electron Transfer. *Acc. Chem. Res.* **2016**, *49*, 2295. (b) Beatty, J. W.; Stephenson, C. R. J. Amine Functionalization via Oxidative Photoredox Catalysis: Methodology Development and Complex Molecule Synthesis. *Acc. Chem. Res.* **2015**, *48*, 1474. (c) Shaw, M. H.; Twilton, J.; MacMillan, D. W. C. Photoredox Catalysis in Organic Chemistry. *J. Org. Chem.* **2016**, *81*, 6898.

15 Metherell A. J.; Ward, M. D. Geometric Isomerism in Coordination Cages Based on Tris-Chelate Vertices: a Tool to Control Both Assembly and Host/Guest Chemistry. *Dalton Trans.* **2016**, *45*, 16096.

16 Cullen, W.; Metherell, A. J.; Wragg, A. B.; Taylor, C. G. P.; Williams, N. H.; Ward, M. D. Catalysis in a Cationic Coordination Cage Using a Cavity-Bound Guest and Surface-Bound Anions: Inhibition, Activation and Autocatalysis. *J. Am. Chem. Soc.* **2018**, *140*, 2821.

17 Delor, M.; Sazanovich, I. V.; Towrie, M; Spall, S. J.; Keane, T.; Blake, A.J.; Wilson, C.; Meijer, A. J. H. M.; Weinstein, J. A. Dynamics of Ground and Excited State Vibrational Relaxation and Energy Transfer in Transition Metal Carbonyls. *J. Phys. Chem. B* **2014,** *118*, 11781.

18 Fagnoni, M.; Protti, S.; Ravelli, D.; Albini, A. Spectroscopic Characterisation of Photoaccumulated Radical Anions: a Litmus Test to Evaluate the Efficiency of Photoinduced Electron Transfer Processes. *Beilstein J. Org. Chem.* **2013**, *9*, 800.

19 Amada, I.; Yamaji, M.; Tsunoda, S.; Shizuka, H. Laser Photolysis Studies of Electron Transfer Between Triplet Naphthoquinones and Amines. *J. Photochem. Photobiol. A Chem.* **1996**, *95*, 27.

20 Karlsson, S.; Boixel, J.; Pellegrin, Y.; Blart, E.; Becker, H.-C.; Odobel, F.; Hammarström, L. Accumulative Electron Transfer: Multiple Charge Separation in Artificial Photosynthesis. *Faraday Discuss.* **2012**, *155*, 233.

21 Brunner, H.; Scheck, T. Neue Optisch Aktive Pyrazolderivate fur die Enantioselektive Katalyse. *Chem. Ber.* **1992**, *125*, 701.

22 Cullen, W.; Turega, S.; Hunter, C. A.; Ward, M. D. pH-Dependent Binding of Guests in the Cavity of a Polyhedral Coordination Cage: Reversible Uptake and Release of Drug Molecules. *Chem. Sci.* **2015,** *6*, 625.

23 Lee, S.-M.; Kowallick, R.; Marcaccio, M.; McCleverty, J. A.; Ward, M. D. A New Route to Mixed Oxo/Arylimido Complexes of Molybdenum(VI) with a Tris(pyrazolyl)borate Co-ligand: Syntheses, Spectroscopic Properties and Ligand-Centred Redox Activity. *J. Chem. Soc., Dalton Trans.* **1998**, 3443.

24 Origin 2017 (OriginLab, Northampton, MA).

25 Snellenburg, J. J.; Laptenok, S. P.; Seger, R.; Mullen, K. M.; van Stokkum, I. H. M. Glotaran: a Java-based graphical user interface for the R package TIMP. *J. Stat. Softw.* **2012**, *49*, 1.

***Table 1**. Summary of redox and photophysical properties of $[Os_4Zn_4(L^{nap})_{12}]Cl_{16}$, $[Os(L^{nap})_3]Cl_2$ and $[Os(L^{me})_3]Cl_2$; obtained in an aerated aqueous solution at RT.*

	Absorption λ_{max}/nm ($10^{-3}\varepsilon$, L mol^{-1} cm^{-1})	Emission λ_{max}/nm[a]	Emission τ/ns (esd) [b]	$E_{1/2}$ (Os^{2+}/Os^{3+}) / V *vs.* SCE[c]
$[Os_4Zn_4(L^{nap})_{12}]Cl_{16}$	400 (sh), 428 (23.5), 512 (7.2), 559 (sh)	638	337(24)	0.75 (60 mV)[d]
$[Os(L^{nap})_3]Cl_2$	398 (sh), 424 (9.3), 513 (2.6), 561 (sh)	636	183(12), 354(17)[e]	0.74 (80 mV)
$[Os(L^{me})_3]Cl_2$	395 (sh), 430 (5.7), 515 (1.5), 565 (sh)	655	97(2), 206(2)[e]	0.63 (60 mV)

[a] Excitation at 550 nm

[b] Obtained using 410 nm, *ca.* 100 ps pulsed excitation

[c] Measured *vs.* Ag/AgCl reference electrode, calculated using $E_{1/2}$(Ag/AgCl) = +0.045 V *vs.* SCE.

[d] Anodic/cathodic peak separation.

[e] Two components consistent with presence of mixture of *fac* and *mer* isomers, see main text and Figs. S3, S4.

***Table 2.** Redox and photophysical properties of the three guest molecules; TCNB, NQ, NN, and their binding constants inside the cage cavity*

	E_{A/A^-} / V *vs.* SCE	*K* (lum) /M^{-1} [d]	*K* (NMR) /M^{-1} [e]	λ_{max} /nm (neutral guest)	λ_{max} /nm (radical anion)	Grow-in and decay for $Os^{3+}/G^{\bullet-}$ state /ps [f]
TCNB	-0.66 [a]	4 x 10^3	3 x 10^3	300, 330 [a]	462 (436, 414, 375, 354) [a]	21 ± 14 (grow-in) 205 ± 60 (decay)
NQ	-0.71 [b]	2 x 10^3	2 x 10^3	340, 440 [b]	390, 550 [b]	13 ± 4 (grow-in) 185 ± 95 (decay)
NN	-0.99 [c]	8 x 10^3	3 x 10^3	340	465, 272 [c]	18 ± 5 (grow-in) 185 ± 75 (decay)

[a] ref. 18

[b] ref. 19

[c] This work (see Fig. S12)

[d] obtained by luminescence titration with **Os•Zn** in water

[e] obtained by NMR titration with $[Co_8(L^{nap})_{12}]Cl_{16}$ in D_2O

[f] the data presented here are averaged over multiple independent fits obtained from analyses of several samples. The spectra presented in the SI are for one individual experiment only.

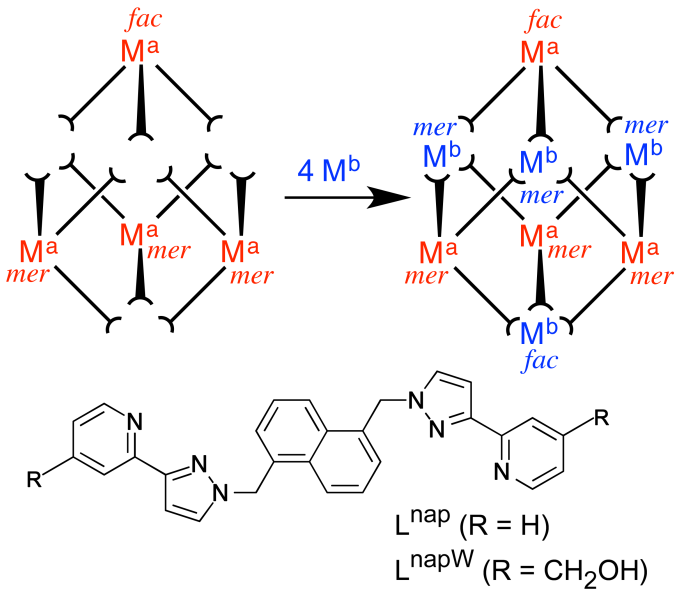

Scheme 1. *The stepwise synthesis of heterometallic cubic cages: combination of four pre-formed, kinetically inert $[(M^a)(L^{nap})_3]^{2+}$ units (M^a = Ru, Os; 1:3 mix of fac and mer isomers) with four labile ions $(M^b)^{2+}$ (M^b = Co, Zn, Cd) to give $[(M^a)_4(M^b)_4(L^{nap})_{12}]^{16+}$. Reproduced from Ref. 10a.*

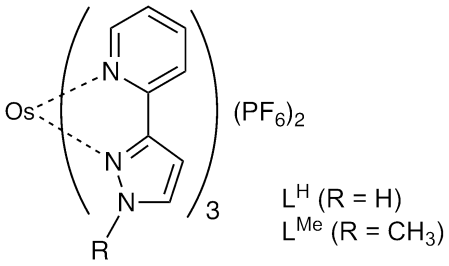

Scheme 2. *Structural formulae of the mononuclear complexes $[Os(L^H)_3](PF_6)_2$ and $[Os(L^{Me})_3](PF_6)_2$ (1:3 mix of fac and mer isomers).*

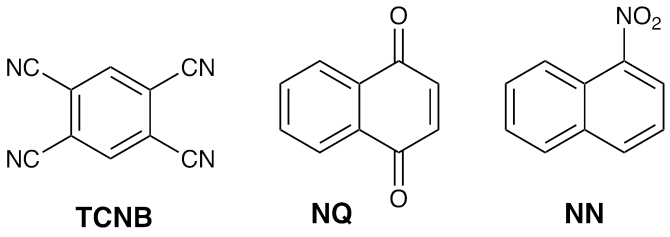

Scheme 3: *Structural formulae of guests used in this work [1,2,4,5-tetracyanobenzene (TCNB), 1,4-naphthoquinone (NQ), and 1-nitronaphthalene (NN)].*

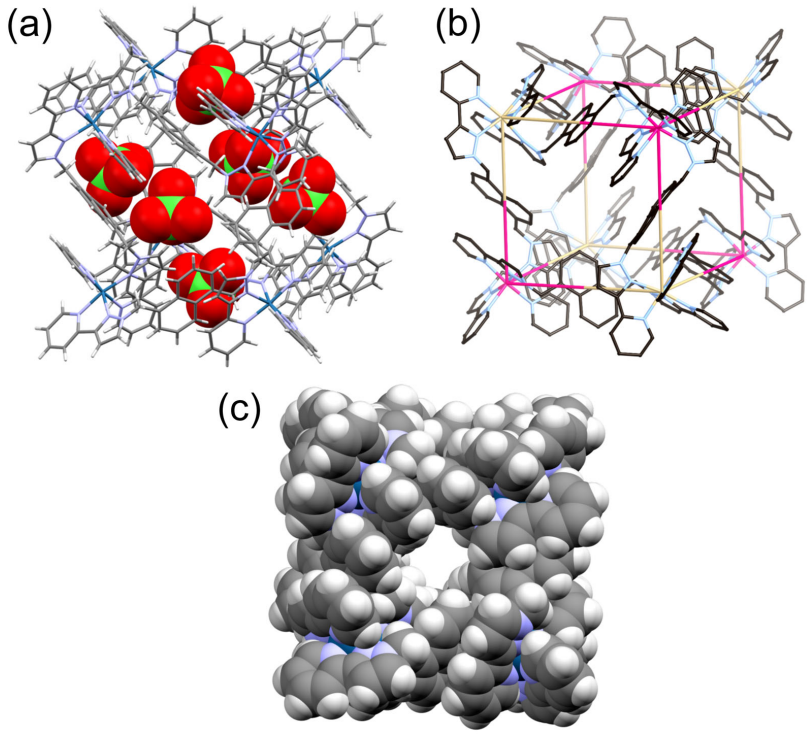

***Figure 1**. Three views of the crystal structure of the complex cation of **Os•Zn** as its perchlorate salt: (a) a view of the whole complex cation (in wireframe) showing the six surface-bound 6 ClO_4^- anions in space-filling mode; (b) a wireframe view of the whole cage emphasising the alternating disposition of two metal ion types in the metal superstructure (red / yellow); and (c) a space-filling view of the complete assembly emphasising the cubic structure and the windows allowing guest access to the central cavity.*

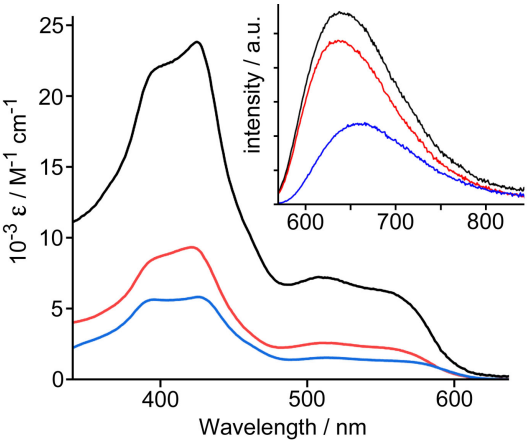

***Figure 2:** UV/Vis absorption spectra of **Os•Zn** (black), $[Os(L^{nap})_3]Cl_2$ (red) and $[Os(L^{me})_3]Cl_2$ (blue), in H_2O. Inset: luminescence spectra of isoabsorbing solutions of **Os•Zn** (black), $[Os(L^{nap})_3]Cl_2$ (red) and $[Os(L^{me})_3]Cl_2$ (blue), in H_2O, with 550 nm excitation.*

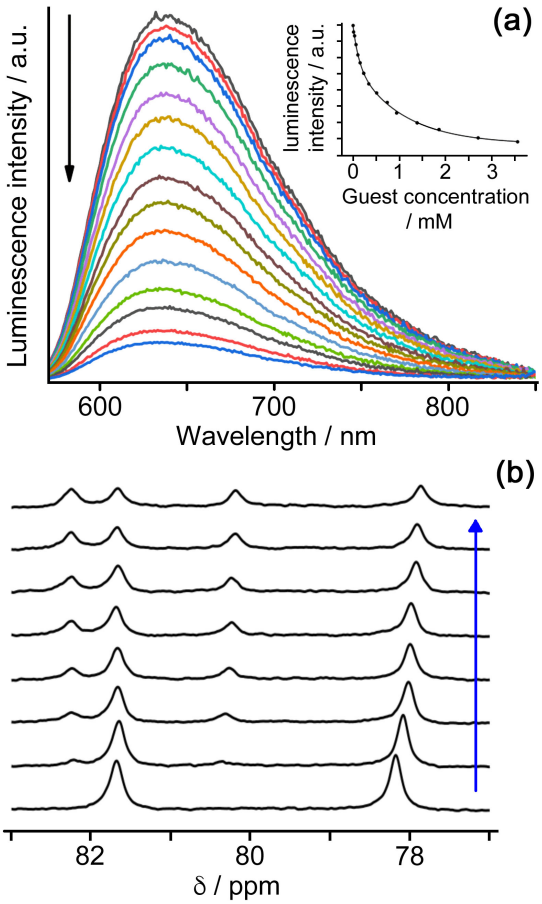

Figure 3: *(a) Luminescence titration of* $[Os_4Zn_4(L^{nap})_{12}]Cl_{16}$ *(0.025mM) with 1,4-naphthoquinone as guest in* H_2O*, using excitation at 550 nm, up to the point at which cage is ca. 90% occupied by guest. (b) NMR titration of the isostructural cage* $[Co_8(L^{nap})_{12}]Cl_{16}$ *(0.15mM) with increasing NQ guest concentration (up to 16 equivalents), in* D_2O*.*

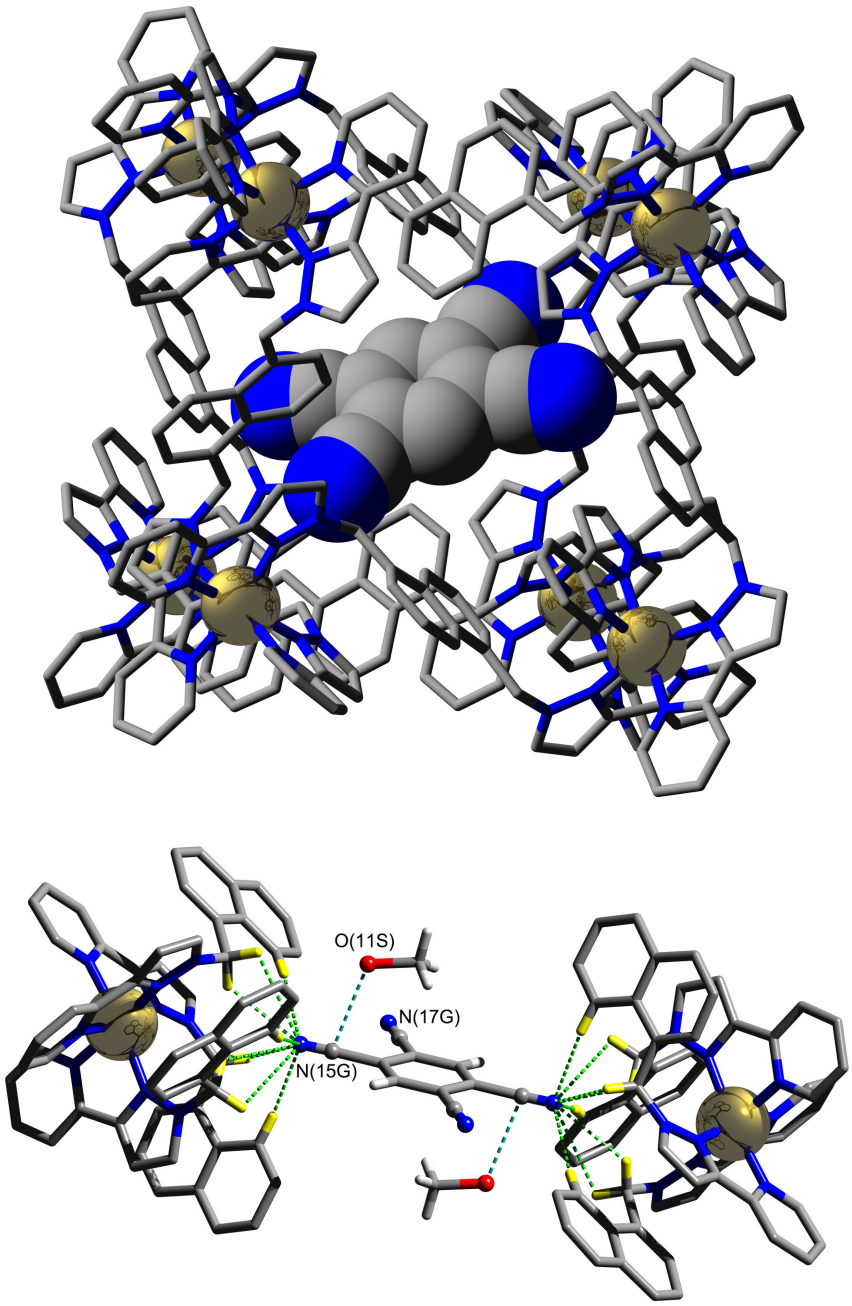

Figure 4: *Two views of the crystal structure of the cage/guest adduct* $[Co_8(L^{nap})_{12}](BF_4)_{16}$•*0.66(TCNB) showing the presence of the bound guest in the cavity of the cage cation* $[Co_8(L^{nap})_{12}]^{16+}$*, which is isostructural with the cage cation of* ***Os•Zn.*** *Top: view of the complete cage (H atoms not included) showing the position and orientation of the guest. Bottom: a view showing the guest and only the two opposed fac-tris(chelate) metal complex vertices that form the hydrogen bond donor pockets, with the collection of inwardly-directed H atoms that participate in CH•••N H-bonding interactions with N(15G) and N(17G) shown in yellow. A short intermolecular distance 2.90(1) Å is apparent between cage-encapsulated methanol oxygen atom O(11S) and the guest cyano carbon atom C14G. The distance and angle [O(11s)•••C(14G)-N(15G), 101.6(3)) are consistent with the Burgi-Dunitz angle describing the approach of a nucleophile to an unsaturated carbon atom (see SI).*

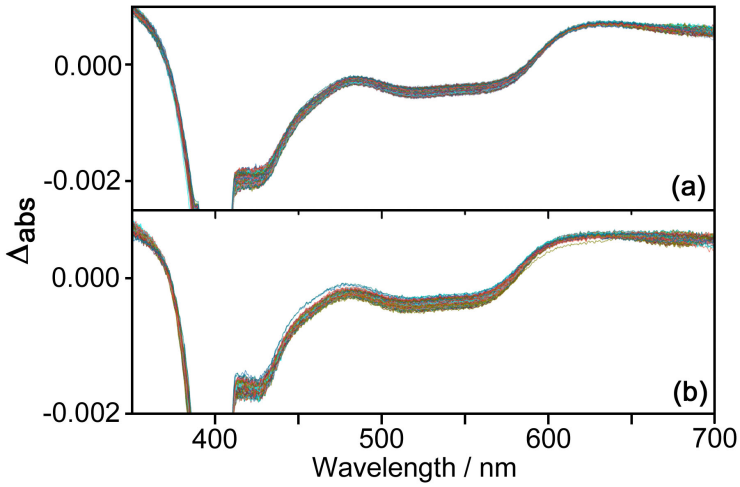

***Figure 5**: Transient absorption spectra at a series of time delays from 1 ps – 5ns in H_2O, following 400 nm, 40 fs pulse excitation for (a) $[Os(L^{me})_3]Cl_2$, (b) **Os•Zn**, illustrating the similarity of their excited-state behaviour.*

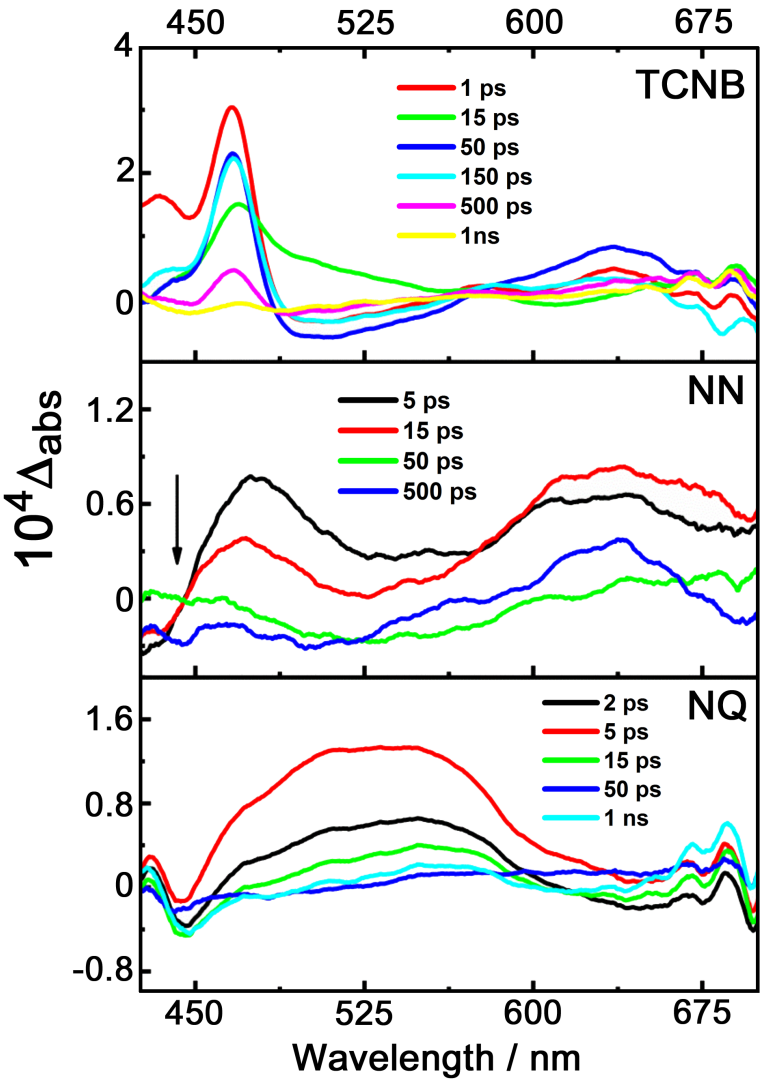

Figure 6. *Transient absorption spectra (400 nm, ~40 fs excitation, in water) obtained by subtracting spectra at selected shorter time delays (5 ps to 1 ns) from a spectrum with a time delay of 5 ns, for the complexes of* ***Os•Zn*** *with the 3 different guests TCNB, NN and NQ.*

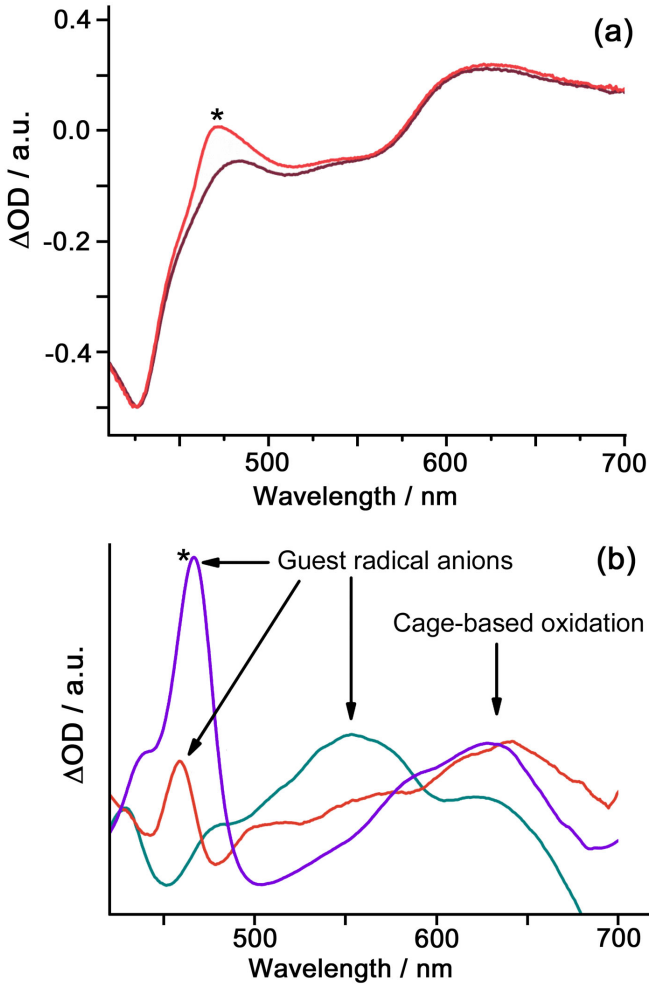

Figure 7. *Transient absorption spectroscopy data obtained under 400 nm, ~40 fs excitation, in water. (a) Decay associated spectra of the* ***Os•Zn****/TCNB complex, with the red line corresponding to the transient spectral features that have a decay constant of 205±60 ps, and brown line corresponding to the transient spectral features of* ***Os•Zn*** *only with a decay constant of 25 ns (long time constant). The asterisk (*) indicates the most prominent spectral feature in the short-lived excited state of* ***Os•Zn****/TCNB that is not present in the longer-lived excited state of* ***Os•Zn****, and corresponds to the main absorption feature of* $TCNB^{\bullet-}$*. (b) The excited-state spectra of each of the three* ***Os•Zn****/guest complex assemblies, obtained by subtracting the spectrum associated with the long decay constant (arising from the free, unquenched* ***Os•Zn*** *that is present in the equilibrium) from the spectrum associated with short decay constant (arising from the* ***Os•Zn****/guest complexes in each case; see Fig. S8) to emphasise the short-lived components (TCNB, purple; NN, red; NQ, green).*

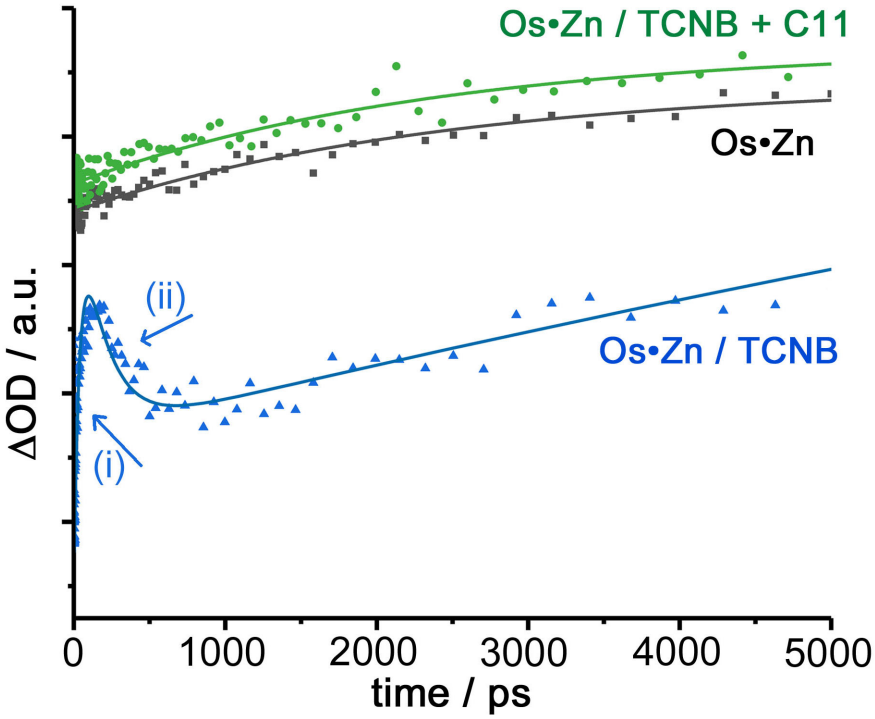

Figure 8. *Excited state decay kinetics obtained from transient absorption spectroscopy data from the* ***Os•Zn****/TCNB complex in water, at 460 nm (averaged over 5 nm). The traces correspond to free* ***Os•Zn*** *(black); the* ***Os•Zn****/TCNB complex [blue, with the obvious appearance of the short-lived transients corresponding to (i) formation and (ii) decay of the charge-separated state (see Table 2 for lifetimes of these, and detailed kinetic data in the SI); and* ***Os•Zn****/TCNB/cycloundecanone (green). The green trace shows the loss of the short-lived grow-in and decay components when the guest, though still present in the mixture, is displaced from the cage cavity by stronger-binding cycloundecanone (C11). At 460 nm both the grow-in and decay of the charge-separated state are particularly clear as this is the absorption maximum of* $TCNB^{\bullet-}$.

Synopsis for Table of Contents

An octanuclear cubic Os_4Zn_4 coordination cage, containing Os(II) tris-diimine units at four of the eight vertices which are good photo-electron donors from their ^{3}MLCT excited state, perform photoinduced electron transfer to electron-accepting organic guests which bind in the central cavity in water *via* the hydrophobic effect: the resulting charge-separated states have lifetimes of *ca.* 200 ps and have been characterised by transient absorption spectroscopy.